Chem

CellPress

Article

Self-activated energy release cascade from anthracene-based solid-state molecular solar thermal energy storage systems

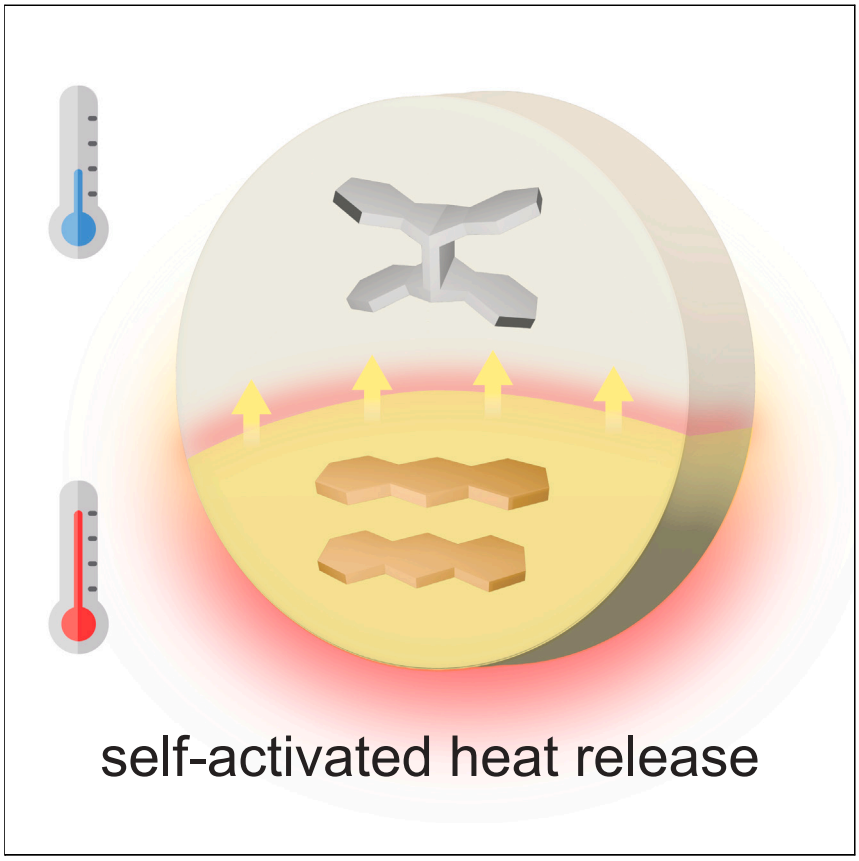

Subhayan Chakraborty, Han P.Q. Nguyen, Junichi Usuba, ..., Klaus Schmidt-Rohr, Jihye Park, Grace G.D. Han

gracehan@brandeis.edu

Highlights

Donor-acceptor anthracenes that undergo [4+4] photocycloaddition are reported

The first observation of self-activated heat release from dianthracenes is achieved

Design principles for solar rechargeable solid fuels are discovered

We discovered donor-acceptor anthracene derivatives that absorb photon energy and store it in strained chemical bonds by dimerizing in the solid state. The compounds exhibit a unique self-activated energy release during their cycloreversion, which addresses a key challenge in extracting the stored energy in molecular solar thermal energy storage systems. This process mirroring the self-ignition of fossil fuels opens up opportunities to use the compounds as effective and renewable solid-state fuels that can release energy rapidly and completely upon initial activation.

Chakraborty et al., Chem *10*, 3309–3322
November 14, 2024
https://doi.org/10.1016/j.chempr.2024.06.033

Chem

CellPress

Article

Self-activated energy release cascade from anthracene-based solid-state molecular solar thermal energy storage systems

Subhayan Chakraborty,[1,3] Han P.Q. Nguyen,[1,3] Junichi Usuba,[1] Ji Yong Choi,[2] Zhenhuan Sun,[1] Cijil Raju,[1] Gustavo Sigelmann,[1] Qianfeng Qiu,[1] Sungwon Cho,[1] Stephanie M. Tenney,[1] Katherine E. Shulenberger,[1] Klaus Schmidt-Rohr,[1] Jihye Park,[2] and Grace G.D. Han[1,4,*]

SUMMARY

We introduce donor-acceptor substituted anthracenes as effective molecular solar thermal energy storage compounds that operate exclusively in the solid state. The donor-acceptor anthracenes undergo a visible light-induced [4+4] cycloaddition reaction, producing metastable cycloadducts—dianthracenes with quaternary carbons—and storing photon energy. The triggered cycloreversion of dianthracenes to anthracenes discharges the stored energy as heat in the order of 100 kJ/mol (200 J/g). The series of compounds displays remarkable self-heating, or cascading heat release, upon the initial triggering. Such self-activated energy release is enabled by the large energy storage in dianthracenes, low activation energy for their thermal reversion, and effective heat transfer to unreacted molecules in the solid state. This process mirroring the self-ignition of fossil fuels opens up opportunities to use dianthracenes as effective and renewable solid-state fuels that can release energy rapidly and completely upon initial activation.

INTRODUCTION

The concept of molecular solar thermal (MOST) energy storage has been largely demonstrated with molecular photoswitches including norbornadienes,[1,2] azo(hetero)arenes,[3–6] hydrazones,[7] dihydroazulenes,[8,9] and fulvalene diruthenium[10,11] derivatives that store photon energy in their metastable photoisomers. Although many of these systems and potential candidates have been primarily investigated in solution state[12–18] and in confined spaces,[19–25] enabling energy storage and release processes in condensed liquid or solid phases has been actively pursued to achieve MOST systems with maximized gravimetric energy densities. In this effort, various azo(hetero)arenes[26–29] and hydrazone[7] derivatives were designed to undergo photo-induced structural changes in solids and transform into liquids, harnessing the additional energy storage from the phase transition. Recently, another class of MOST compounds has emerged, which stores photon energy via crystalline-state photochemical reactions,[30–34] showcased by the intermolecular [2+2] photocycloaddition among styrylpyryliums.[35] The strong donor-acceptor design of styrylpyrylium (STP) structures allowed for the favorable head-to-tail stacking of molecules in crystals and the facile [2+2] cycloaddition upon the absorption of a broad range of visible light as well as the natural solar spectrum. Also, both UV-induced and thermally activated cycloreversion of cyclobutanes to styrylpyryliums were successful, releasing the stored energy as heat ($\Delta H_{storage}$).

THE BIGGER PICTURE

The sun being our greatest source of renewable energy, scientific developments focus on tactically storing the sunlight and purposefully using it in the right energy form. Over time, many organic photoswitches have emerged as molecular solar thermal (MOST) energy storage materials to harness the photon energy of sunlight and release thermal energy on demand. However, many photoswitches demand large molecular motions for isomerization, which is highly obstructed in a solid phase, limiting practical applications. We demonstrate a set of donor-acceptor functionalized anthracene derivatives that undergo photocycloaddition to dianthracenes and subsequently release heat during their cycloreversion, all in the solid state. The heat release is self-activating, which solves one of the biggest challenges in the effective utilization of MOST compounds, i.e., the difficulty in extracting the stored energy. The new compounds are anticipated to serve as rechargeable and easy-to-use solid-state fuels.

Although this demonstration highlighted the opportunities to use solid-state intermolecular photochemical reactions for MOST energy storage, there were significant limitations of the styrylpyrylium-based systems. First, the maximum energy storage density of 42 kJ/mol per cyclobutane and gravimetric energy density of 51 J/g[35] were suboptimal compared with the conventional MOST systems such as azo(hetero)arenes[36,37] and norbornadienes[38–40] that offer energy storage densities over 100 kJ/mol and 300 J/g. Second, the activation energy ($\Delta G^{\ddagger}$) of 121–122 kJ/mol for the thermally activated cycloreversion process is far greater than the released energy of 42 kJ/mol, which necessitates the continuous heating of the metastable cyclobutanes at temperatures above 131°C for complete cycloreversion and heat release.[35] Therefore, the energy release could be monitored only on a few-milligram scale using differential scanning calorimetry (DSC), while it was challenging to detect any sizable temperature increase of the solid MOST compounds outside the thermally insulated environment of DSC. The small amount of energy released from the solids quickly dissipates to the air and substrates, leading to negligible temperature changes of the compounds that are in thermal equilibrium with the heat source.

For any potent fuels, the ability to self-heat upon initial triggering is essential, which limits the external energy supply to a short-term initiation and maximizes the efficiency of energy release. For example, the self-ignition of hydrocarbons enables the complete and spontaneous combustion of the fuels after the initial compression[41]- or electrical discharge-induced triggering of the exothermic reactions.[42,43] Frontal polymerizations have also leveraged exothermic reactions to self-propagate the polymer growth.[44–47] These irreversible self-activating reactions generate products such as carbon dioxide, water, and polymers.[41–47] To the best of our knowledge, any significant self-activated energy release from MOST systems has not been observed for several reasons. In solution state, heat dissipation to the large volume of solvent is prominent and restricts effective heat transfer to the unreacted metastable isomers. Even in the solid state, thin films or powders have large surface areas where the released heat quickly dissipates to the surroundings, limiting the heat transfer between molecules.[48,49] Lastly, the $\Delta G^{\ddagger}$ for thermal reversion is generally much greater than the released energy per molecule, which fundamentally prevents a cascade of exothermic reactions.[35,50,51]

Thus, we aim to design scalable MOST systems that operate in solvent-free conditions, store a large quantity of energy ($\Delta G_{storage}$), comparable to or greater than the $\Delta G^{\ddagger}$ of reversion, and self-activate the heat release and propagation. In order to improve the $\Delta G_{storage}$, we selected a small and neutral aromatic molecule, anthracene, as a scaffold for MOST energy storage compounds. The molecular weight of anthracene (178 g/mol) is significantly smaller than that of styrylpyryliums (412–474 g/mol) bearing two *t*Bu groups and heavy counter-anions ranging from BF_4^- and ClO_4^- to $CF_3SO_3^-$.[35] The solid-state photodimerization of anthracenes has been largely studied for their photomechanical responses in crystals,[52] particularly with those bearing a Me[53–56] or a COOH[57–60] group on the 9-position of anthracene. Anthracenes have also been incorporated into the building blocks of covalent organic frameworks[61–63] and metal organic frameworks,[64,65] displaying reversible dimerization in solid state. The potential of anthracene derivatives for MOST energy storage has been studied only at a fundamental level[66–70]; anthracenes bearing a functional group (CHO, CH_2OH, Me, and longer alkyls) on the 9-position[71–75] or two groups (OMe and COOR) on 2,6-positions[76] were photodimerized in solutions, and their thermal reversion was monitored either in solutions or in molten liquid states, recording small energy storage values of 20–30 kJ/mol.

[1]Department of Chemistry, Brandeis University, 415 South Street, Waltham, MA 02453, USA

[2]Department of Chemistry, University of Colorado Boulder, 215 UCB, Boulder, CO 80309, USA

[3]These authors contributed equally

[4]Lead contact

*Correspondence: gracehan@brandeis.edu

https://doi.org/10.1016/j.chempr.2024.06.033

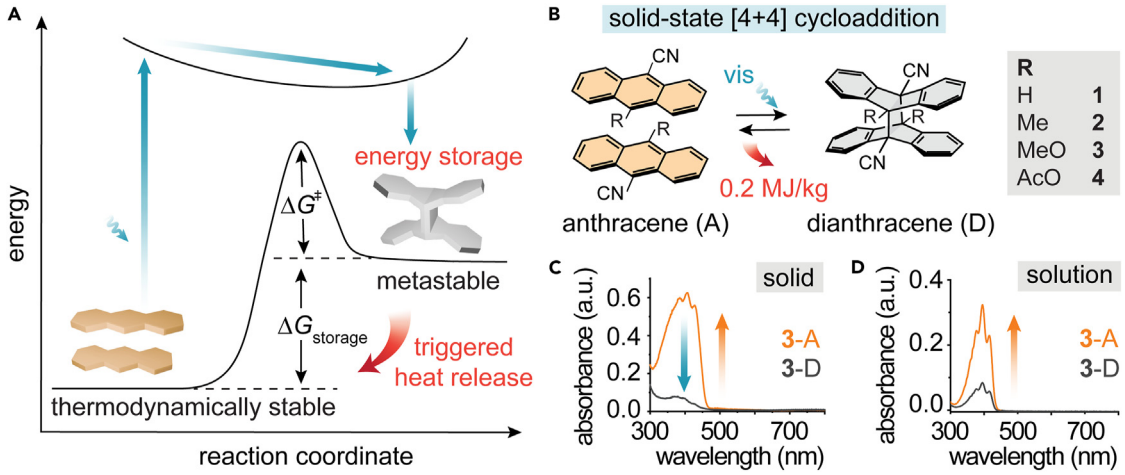

Figure 1. Energy storage and release via reversible cycloaddition of anthracenes

(A) Schematic illustration of photon energy storage in dianthracenes and triggered release of energy during their cycloreversion to anthracenes.

(B) Reversible [4+4] cycloaddition of anthracene derivatives **1**–**4**.

(C) Solid-state UV-vis absorption spectra of **3**-A and **3**-D obtained from irradiation and thermal reversion.

(D) Solution-state UV-vis absorption spectra of **3**-A and **3**-D in dichloromethane. **3**-A is obtained from the thermal reversion of **3**-D in solution.

However, a report in 1972 by Donati et al. illustrated rare exceptions; the dimers of 9-CN-anthracene and 9-CN, 10-AcO-anthracene were revealed to undergo solid-state thermal cycloreversion to anthracenes, releasing 74 and 82 kJ/mol, respectively.[77] The temperatures of thermal reversion were lower than the melting points of the corresponding anthracenes, enabling the measurement of the enthalpy associated with the solid-to-solid transition. Building upon this observation, we hypothesized that 9-CN-anthracene derivatives could be good candidates for MOST energy storage, upon the functionalization of the 10-position, which fine-tunes the relative scale of $\Delta G^{\ddagger}$ of thermal reversion and $\Delta G_{storage}$. The successful elucidation of the structure-property relationships would enable the self-activated energy release from dianthracenes in solid state.

RESULTS AND DISCUSSION

To understand the significance of substituents on anthracenes for energy storage, we initially performed a theoretical investigation of $\Delta G_{storage}$ among the anthracene derivatives bearing various electron-donating and -withdrawing functional groups (Me, MeO, Br, CN, and NO_2) on the 9-position. Our density functional theory (DFT) calculation results suggest that there is a large gap between the $\Delta G_{storage}$ of 9-CN-anthracene (106 kJ/mol) and the rest of anthracene derivatives (51–65 kJ/mol) (Table S1). Additionally, varying the functional group position on anthracene results in a larger $\Delta G_{storage}$ value for 9-CN than 1-CN and 2-CN (54 and 42 kJ/mol, respectively) (Figures S1–S3). Based on these results, we postulate that the 9-CN functionalization significantly stabilizes the anthracene structure via effective electron delocalization, relative to the dearomatized dianthracene counterpart with considerably less electron delocalization, increasing the energy gap between the two states. Thus, we designed and investigated anthracene derivatives with donor-acceptor structures, which would further enhance the electron delocalization over the anthracene structures and potentially increase $\Delta G_{storage}$.

Functionalized anthracenes undergo [4+4] photodimerization in the solid state (Figure 1A) when the distance between two neighboring, cofacial reactive units is within 4.2 Å, according to Schmidt's principle.[78] The resulting dianthracenes are

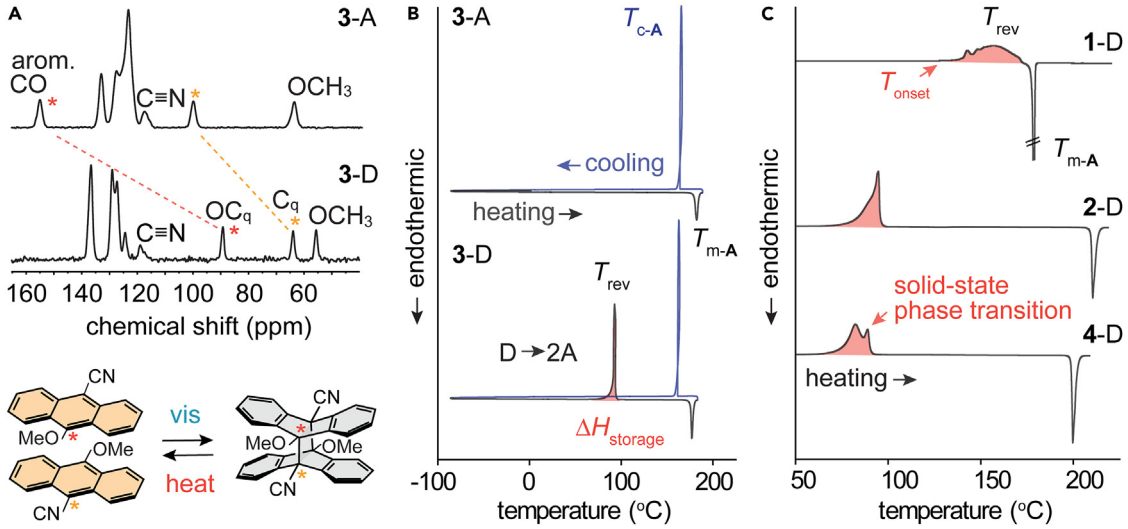

Figure 2. Solid-state characterizations

(A) Solid-state ^{13}C NMR spectra of **3**-A and **3**-D and the corresponding chemical structures.

(B) DSC thermograms of **3**-A and **3**-D measured during the first heating (black) and cooling (blue) cycle.

(C) DSC thermographs of **1**-D, **2**-D, and **4**-D, measured during the first heating cycle. Red highlighted areas represent the exotherms of cycloreversion ($\Delta H_{storage}$). $T_{m\text{-}A}$, melting point of anthracene; $T_{c\text{-}A}$, crystallization point of anthracene; T_{rev}, peak temperature of thermal reversion; T_{onset}, onset temperature of thermal reversion.

metastable, storing the energy equivalent to the difference between the thermodynamically stable anthracene pairs and dianthracenes ($\Delta G_{storage}$). Upon thermal or photochemical triggering, the cycloreversion to anthracenes occurs, releasing the $\Delta H_{storage}$. DSC allows for the measurement of $\Delta H_{storage}$, which can be a good approximation for $\Delta G_{storage}$, for solid-state cycloadditions that undergo minimal structural and volume changes compared with solution- or gas-phase reactions. We investigated 9-CN-anthracene derivatives by functionalizing the 10-position with H (**1**), Me (**2**), MeO (**3**), and AcO (**4**) (Figure 1B). In addition to increasing the electron delocalization over anthracenes, the donor-acceptor structures are expected to facilitate a head-to-tail stacking of the monomers in the crystals, which increases the chance of dimerization and yielding a single isomer of the photodimer. We prepared photodimers of compounds **1**–**3** via irradiation with a 405 nm LED in the solid state; the anthracenes were mixed and stirred with small stainless-steel balls in a stainless-steel jar, assisted by magnetic stirring (Video S1). The ball-mixed solid-state photodimerization was quantitative and more effective than the photoconversion of static or solvent suspended powder samples (Figures S4–S7; Table S2). Compound **4** was able to photodimerize only in ether suspension, indicating the less favorable packing of anthracenes and limited conformational freedom in crystals. The UV-vis absorption spectra of compounds **1**–**3** were recorded in thin films (Figures 1C and S8–S11) that showed reversible dimerization upon photoirradiation and thermal activation. For compound **4**, diffuse reflectance spectra were acquired instead, due to the difficulty of obtaining uniform films for the dianthracene (Figure S8). In solutions, the dianthracenes rapidly revert to anthracenes even at room temperature (Figure 1D), and the photocycloaddition of anthracenes in solution was not performed because it could produce a mixture of head-to-head and head-to-tail dimers. All UV-vis absorption spectra of solution-state compounds are illustrated in Figure S12.

The formation of dianthracenes in high yield was confirmed by solid-state nuclear magnetic resonance (NMR) spectroscopy (Figure 2A). Since dianthracenes readily

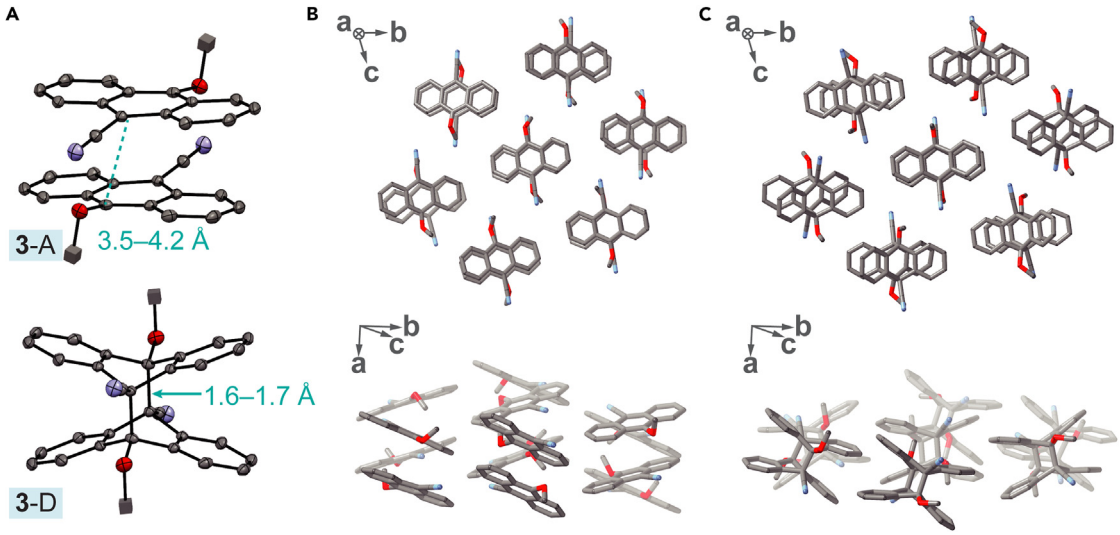

Figure 3. Simulated crystal structures of 3-A and 3-D

(A) Simulated and refined crystal structures of **3**-A and **3**-D, showing head-to-tail stacking of anthracenes and the shortened distance between reactive carbons upon bond formation. Simulated and refined packing structures of (B) **3**-A and (C) **3**-D, displaying crystal-to-crystal transformation and 0.3% volume increase upon dimerization.

revert to the monomer anthracenes upon dissolution in organic solvents, it is difficult to identify the chemical composition of the as-synthesized dianthracenes using solution-state NMR (Figures S13–S25). The solid-state ^{13}C NMR spectra of all dianthracenes show >97% dimer content with negligible monomer residue, and the different chemical shifts of the reactive carbon atoms before and after dimerization are clearly monitored (Figures S26–S29). Thermal properties of anthracenes and dianthracenes were investigated using DSC in the range from −90°C to around 200 °C, below their decomposition temperatures (Figure S30). The anthracenes exhibit clear melting and crystallization, and the dianthracenes undergo exothermic thermal cycloreversion to generate corresponding anthracenes, allowing for the measurement of $\Delta H_{storage}$ that serves as an approximation for $\Delta G_{storage}$ (Figures 2B and S31). The heating curves of all dianthracenes are illustrated in Figures 2B and 2C, showing multiple exothermic events occurring simultaneously. Typical energy release from metastable MOST compounds such as azo(hetero)arenes,[37] hydrazones,[7] Lewis acid-coordinated azo compounds,[29] and styrylpyryliums,[35] appears as a broad exotherm resembling a Gaussian curve. The presence of sharp peaks in addition to the broad exotherm indicates that additional exothermic process(es) accompanies the thermal cycloreversion. We hypothesize that crystal-to-crystal phase transition occurs during the cycloreversion, which contributes to the large $\Delta G_{storage}$ values of 9-CN-anthracene derivatives.

Crystal structures were analyzed using the combination of single-crystal X-ray diffraction (XRD) (**1**-A, **1**-D, and **2**-A) and structure simulation from powder XRD (PXRD) data, refined by Pawley method (**2**-D, **3**-A, **3**-D, **4**-A, and **4**-D) (Tables S3 and S4; Figures S32 and S33). Figure 3A shows the head-to-tail stacked **3**-A pairs displaying distances between the reactive carbon atoms below 4.2 Å, fulfilling Schmidt's principle. The photoirradiation of **3**-A crystals generates head-to-tail dimer **3**-D, while inducing small changes in molecular packing. Figures 3B and 3C show the overall crystal structure changes between **3**-A and **3**-D, with about 0.3% of unit cell volume increase upon dimerization. The crystal structures of all monomers and dimers of compounds **2**–**4** are illustrated in Figures S34–S41, documenting

Table 1. Thermal parameters for cycloreversion process

D→A	$T_{m\text{-}A}$ (°C)	T_{onset} (°C)	$\Delta G_{storage}$ (kJ/mol)	$\Delta G_{storage}$ (J/g)	$\Delta G^{\ddagger}$ (kJ/mol)	$t_{1/2}$ (days)
1	179	140	82	201	129	69,543
2	207	68	96	221	107	5.7
3	176	75	96	205	104	6.3
4	197	59	102	195	101	1
STP	250	132	42	51	122	2,045

$T_{m\text{-}A}$, melting point of anthracene monomer; T_{onset}, onset temperature of cycloreversion; $\Delta G_{storage}$, energy storage density; $\Delta G^{\ddagger}$, activation energy for thermal cycloreversion in solid state; $t_{1/2}$, thermal half-life of dianthracene at room temperature in solid state.

unit cell volume changes of 4% (**2**) and 3% (**4**) upon dimerization. Compound **1** undergoes the most significant structural changes from **1**-A (head-to-head paired) to **1**-D (head-to-tail dimer) and a space group change, indicating the rotation of anthracenes under photoirradiation during the dimerization process.[79] Based on the changes of the molecular packing for compounds **1–4** upon dimerization, we recognize the contribution of the solid-state phase transition enthalpies to the overall energy storage densities of these MOST systems.

Table 1 summarizes the important thermal parameters relevant to the cycloreversion process of compounds **1–4** and a styrylpyrylium that exhibited the greatest energy storage for the [2+2] cycloaddition-based MOST system. First, we compare the melting points of anthracenes ($T_{m\text{-}A}$) and the onset temperature for thermal cycloreversion (T_{onset}) recorded by DSC. For all compounds, $T_{m\text{-}A}$ is higher than T_{onset}, which is critically important for achieving a net exothermic process of cycloreversion. If $T_{m\text{-}A}$ is similar to or lower than T_{onset}, the released heat is reabsorbed during the melting process of the generated anthracenes, significantly reducing the overall energy release. We notice that T_{onset} values of donor-acceptor structures **2–4** are substantially lower than that of 9-CN-anthracene (**1**), which favorably increases the temperature gap between T_{onset} and $T_{m\text{-}A}$ and prevents the reabsorption of thermal energy by the melting of anthracene. The lower T_{onset} values also indicate the smaller $\Delta G^{\ddagger}$ of cycloreversion for compounds **2–4**, achieved by the functionalization at the 10-position (*vide infra*).

All compounds **1–4** display substantial energy storage densities ($\Delta G_{storage}$), both per molecule and per mass, comparable to those of norbornadienes[39,40] and phase-transition MOST compounds based on azo(hetero)arenes (Figure S42).[26,37] These values of up to 102 kJ/mol or 221 J/g, significantly larger than those of styrylpyryliums (max. 42 kJ/mol or 51 J/g),[35] are attributed to the intrinsically weaker and longer C–C bonds of dianthracenes (1.61 Å for STP dimer,[35] 1.63–1.65 Å for **1**-D[80]) and the additional exothermic events associated with solid-state phase transitions. We also measured the Gibbs free energy of activation ($\Delta G^{\ddagger}$) and half-lives for the thermal cycloreversion of dianthracenes using DSC (Figures S43–S46; Table S5). Notably, the $\Delta G^{\ddagger}$ and $\Delta G_{storage}$ values of dianthracenes were nearly identical for **4**-D and similar for **2**-D and **3**-D (Table 1), in contrast to styrylpyryliums that exhibit much greater $\Delta G^{\ddagger}$ than $\Delta G_{storage}$ (~3 times). We have compiled $\Delta G^{\ddagger}$ and $\Delta G_{storage}$ values of reported MOST energy storage systems (Figure S42) to find that the majority of such systems display much greater $\Delta G^{\ddagger}$ than $\Delta G_{storage}$. Thus, we hypothesize that this modest difference between $\Delta G^{\ddagger}$ and $\Delta G_{storage}$ would allow for the self-activated cycloreversion upon the initial triggering of dianthracenes, as long as the released heat is effectively transferred to the neighboring unreacted dianthracenes.

To verify this hypothesis, we performed local Thermal-triggering experiments on compact solid pellets of compounds (Figure 4A). The temperature profiles of

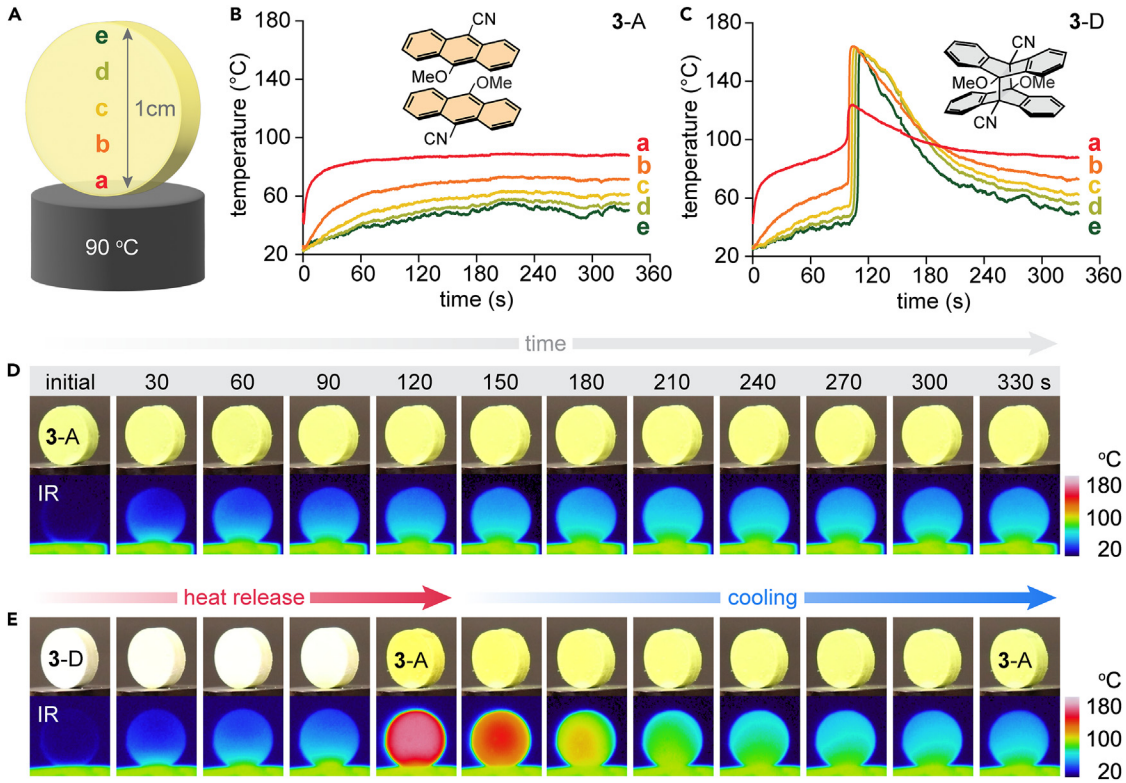

Figure 4. Thermal activation of 3-A and 3-D in pellets

(A) Schematic of the experimental setup composed of a heating block and a solid pellet of compound. Temperature profiles of a solid pellet measured over time at five positions (**a–e**) for (B) **3**-A and (C) **3**-D, and the corresponding images showing the color and temperature change of a pellet over time for (D) **3**-A and (E) **3**-D that reverts to 3-A.

monomeric anthracenes (exemplified with **3**-A in Figure 4B) represent the slow and stagnating heat conduction through the solid organic compounds (Video S2). By contrast, the pellet of dimeric **3**-D undergoes a rapid temperature increase within 2 min of local thermal triggering at position **a**, and the released heat is quickly transferred to positions **b–e**, resulting in a sharp increase in temperature throughout the whole pellet and reaching a maximum temperature of 165°C (Video S3). After the heat release process, the pellet spontaneously cooled down to the baseline temperature via heat dissipation to the surroundings, consistent with the temperature of **3**-A. The abrupt increase in temperature for the pellet of **3**-D, far exceeding the baseline temperature, is attributed to the exothermic process of [4+4] cycloreversion of dianthracenes. To the best of our knowledge, this is the first experimental observation of such a cascade of thermally triggered exothermic processes throughout MOST compounds. A prior report on a solid-state MOST system, consisting of an azobenzene polymer, illustrated the Thermal-triggering experiment for a polymer pellet, which required heating the entire pellet to 150°C using an external heat source.[49] The released heat from the polymer yielded relatively small temperature differences (max. 10°C) from the baseline, due to the small $\Delta G_{storage}$ (less than 100 J/g) and fast thermal equilibrium with the heat source set at the high temperature. Most importantly, no heat cascade has been observed, which makes the donor-acceptor 9-CN-anthracene derivatives a unique class of MOST compounds that can self-activate the heat release from the entire solid materials upon the initial triggering. The optical and infrared radiation (IR) images of pellets of **3**-A and **3**-D are shown in Figures 4D and 4E, corresponding to the temperature profiles in Figures 4B and 4C.

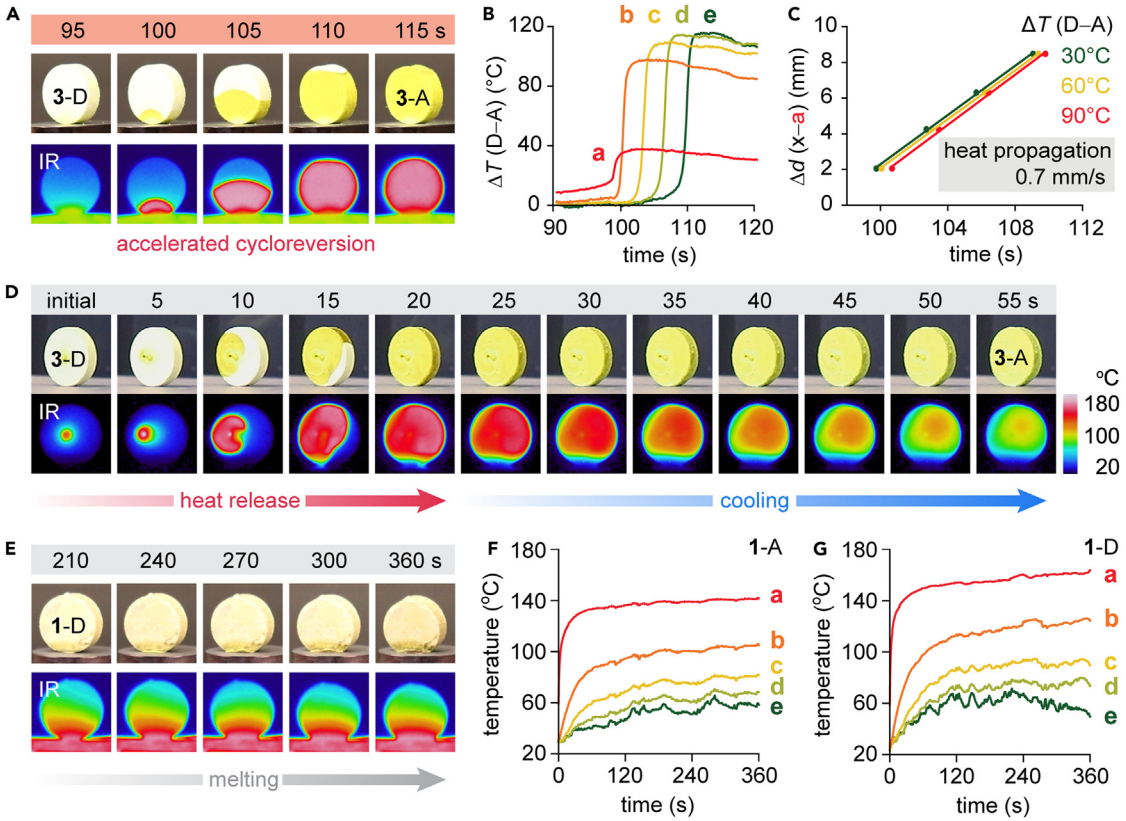

Figure 5. Thermal and IR-laser triggering of 3-D and unsuccessful cascade of cycloreversion for 1-D

(A) Optical and IR images showing the color and temperature change of a pellet of **3**-D during heat propagation.

(B) Net temperature increases of the pellet over time (positions **a**–**e** are consistent to those in Figure 4A).

(C) Kinetics of spatial heat propagation. Δ*d* (x–**a**) is the distance between a position on the pellet (**b**–**e**) and the position **a**.

(D) IR-laser triggered cycloreversion and heat cascade for a pellet of **3**-D.

(E) Optical and IR images showing the melting process of a pellet of **1**-D upon cycloreversion.

(F and G) Temperature profiles of a solid pellet measured over time at five positions (**a**–**e**) for (F) **1**-A and (G) **1**-D.

To investigate the rapid heat cascade process, we analyzed the propagation of heat front through the pellet (Figure 5A). The bottom of the pellet (position **a**) starts to release heat at 100 s, and the heat transfer to the top of the pellet (position **e**) is completed within 10 s (Figure 5B). The net temperature change of the pellet, achieved by the exothermic cycloreversion, is shown as Δ*T* (D–A) and is as large as 120°C, underlining the enormous potential of the MOST system as a renewable heating material for a thermal battery application. The rate of spatial heat propagation (v_{prop}) through the solid pellet is measured to be 0.7 mm/s for compound **3** (Figure 5C), and the successful observation of self-activated heat release for compounds **2**–**4** is summarized in Table 2 and illustrated in detail in Figures S47–S51. Videos S4, S5, S6, and S7 show the heating experiments of compounds **2**-A, **2**-D, **4**-A, and **4**-D, respectively. The induction period for thermal triggering (t_{ind}) is even shorter, and v_{prop} is higher for compound **4**, due to its lower $\Delta G^{\ddagger}$ value for cycloreversion and more facile heat release compared with **3**. For compound **2**, its low T_{onset} and large $\Delta G_{storage}$ enable a rapid cascade of reversion throughout the pellet, despite its high $\Delta G^{\ddagger}$ value. The maximum temperature detected on each pellet (T_{max}) is also higher for compounds **2** and **4** than compound **3**, highlighting the tunability of the temperature profile and heat release kinetics by molecular design. Since there are significant gaps between the thermal reversion temperature (T_{rev}) and $T_{m\text{-}A}$ for compounds

Table 2. Thermal parameters for the self-activated heat cascade process

D→A	T_{rev} (°C)	T_{trig} (°C)	t_{ind} (s)	v_{prop} (mm/s)	T_{max} (°C)	$T_{m\text{-}A}$ (°C)	$\Delta G_{storage}$ (J/g)
1	156	155	n/a	n/a	166	179	201
2	95	90	83	1.2	185	207	221
3	95	90	96	0.7	165	176	205
4	82	80	76	1.3	174	197	195

T_{rev}, peak temperature of cycloreversion; T_{trig}, triggering temperature set for the heat source; t_{ind}, induction period for thermal triggering; v_{prop}, rate of spatial heat propagation; T_{max}, maximum temperature detected on each pellet; $T_{m\text{-}A}$, melting point of anthracene monomer; $\Delta G_{storage}$, energy storage density.

2–4, the released heat from cycloreversion is not reabsorbed by the melting process of the resulting anthracenes. We note that the pellets of compounds **2** and **4** undergo noticeable shape changes to vertical ovals upon the self-activated heat release (Figures S47 and S48), which is attributed to the larger volume change of compounds **2** and **4** (4% and 3%, respectively) than compound **3** (0.3%) during the cycloreversion. The compounds were tested for the repeated photodimerization and self-activated heat release processes, revealing no degradation by the NMR analysis. The exceptional stability of the compounds under photoirradiation is attributed to the solid-state reaction conditions that limit any side reactions such as the oxidations. The precisely arranged anthracene pairs in crystals undergo facile dimerization, and the exposure to oxygen in crystals is significantly lower than that for dissolved molecules in solutions.

We also designed IR-laser-triggering experiments on pellets of **3**-D (Figure 5D) to confirm that short-term triggering of a smaller area on the pellets can lead to heat propagation. An IR-laser (λ of 1,200 nm, power of 630 mW, and approximate spot size of 29 μm) was used to trigger an off-center position of the pellet of **3**-D for 6–8 s, which resulted in the radial propagation of a heat front and the completion of heat release within 20 s (Video S8; laser irradiation on **3**-A can be seen in Video S9). The similarity in the heat propagation kinetics triggered by the transient laser irradiation and by the heat conduction from a localized heat source indicate that only localized and short-term thermal triggering is necessary to convert a small portion of the MOST materials above a threshold, which is followed by the self-cascading heat transfer and complete conversion. We also designed an experiment where the heated pellet is in contact with a steel plate, a thermally conductive material (Figure S52; Video S10). Due to the rapid heat transfer to the steel plate, the self-activated heat release within the pellet was suppressed. When the steel plate was removed, the cascade of reversion was resumed, which confirms the hypothesis that a threshold has to be reached to initiate the propagation of reaction. Another experiment where the self-activated pellet is submerged in water also stopped the cascade (Figure S52; Video S11), evident from the partially converted pellet, due to the rapid heat dissipation to water.

We note that compound **1**, unlike compounds **2–4**, fails to undergo self-activated heat release, due to the small gap between T_{rev} and $T_{m\text{-}A}$ (Table 2), which leads to the melting of anthracenes by the released heat (Figure 5E; Video S12). The temperature profiles of the pellet of **1**-D do not display any peaks or heat propagation features, similar to those of **1**-A (Figure 5F; Video S13), as a result of the reabsorption of heat by melting of anthracene (Figure 5G). Based on the contrast between the unsuccessful (**1**) and successful (**2–4**) heat release experiments, we conclude that the temperature gap between T_{rev} and $T_{m\text{-}A}$ should be at least 80°C to prevent the undesirable melting of anthracenes for the size of pellets we tested (300 mg, 1 cm in diameter).

A

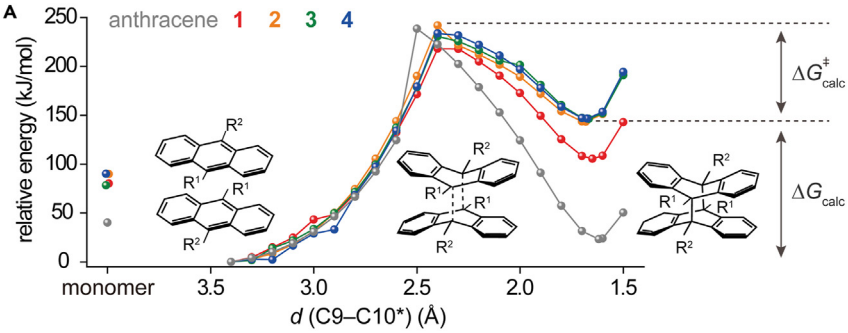

B

	ΔG_{calc} (kJ/mol)	$\Delta G^{\ddagger}_{calc}$ (kJ/mol)	d (C9–C10*)$_D$ (Å)	d (C9–C10*)$_{TS}$ (Å)
anthracene	28	211	1.619	2.5
1	109	113	1.649	2.4
2	143	98	1.682	2.4
3	146	84	1.667	2.4
4	146	87	1.675	2.4

Figure 6. DFT calculation of [4+4] cycloaddition process

(A) DFT calculation results on [4+4] cycloaddition and reversion of anthracene derivatives, showing energy level changes surveyed as the distance between two cofacial anthracenes was varied, calculated at the B3LYP-D3/6-31+G(d,p) level of theory.

(B) Table summarizing the calculation results. ΔG_{calc}, calculated energy storage density; $\Delta G^{\ddagger}_{calc}$, calculated activation energy; d (C9–C10*)$_D$, distance between a 9-position of an anthracene and a 10-position of the counterpart in a dimer; and d (C9–C10*)$_{TS}$, distance between a 9-position of an anthracene and a 10-position of the counterpart in a transition state.

Lastly, we performed a theoretical investigation of the energetic changes during the cycloreversion of dianthracenes. We first defined d (C9–C10*) as the distance between a 9-position of an anthracene and a 10-position of the counterpart in a dimer or monomer pair. While changing the d (C9–C10*) by 0.1 Å in the range from 1.5 to 3.4 Å, we performed the structural optimization of the paired molecules (Figure 6A). The most energetically stable structure within this range was obtained at d (C9–C10*) of 3.4 Å for each compound, so the energy of this structure was used as a reference point. Compounds **1**–**4** display the maximum relative energy when d (C9–C10*) equals 2.4 Å, and we assigned the corresponding structures to the approximated transition states.[81] The results suggest that the introduction of 9-CN and electron-donating groups on the 10-position increases $\Delta G_{storage}$ and decreases the $\Delta G^{\ddagger}$ of thermal cycloreversion, corroborating the experimental observations (Figure 6B). Consistent with our observation of the relative $\Delta G_{storage}$ among 1-CN, 2-CN, and 9-CN anthracenes (Figures S1–S3), compounds **2**–**4** that undergo a large reduction in the effective conjugation upon dimerization display larger $\Delta G_{storage}$ compared with anthracene and compound **1**. We hypothesize that the relatively destabilized dimers **2**–**4** would undergo facile thermal cycloreversion, exhibiting lower $\Delta G^{\ddagger}$ values.

Conclusions

The design of donor-acceptor substituted anthracenes is revealed to be an effective strategy for enhancing the energy storage in dianthracenes upon photocycloaddition. The cycloreversion of dianthracenes releases substantial energy, which is attributed to both the significant change in the conjugation of molecules and their phase transition during the solid-state reaction. The released energy is comparable to the $\Delta G^{\ddagger}$ of thermal reversion, facilitating the self-activation of further cycloreversion

upon initial triggering. Although being similar to conventional fossil fuels that undergo self-ignition and spontaneous combustion, the dianthracenes release heat by self-activation and are recharged by irradiation. The solid-state MOST energy storage system that requires minimal energy input for triggering significantly enhances the efficiency of heat release, and we anticipate further development of diverse condensed-phase MOST energy storage systems that are fine-tuned to achieve such self-activated energy release.

EXPERIMENTAL PROCEDURES

Resource availability

Lead contact

Further information and requests for resources should be directed to and will be fulfilled by the lead contact, Grace G.D. Han (gracehan@brandeis.edu).

Materials availability

Any unique materials generated in this study are available from the lead contact with a completed material transfer agreement.

Data and code availability

Crystallographic data have been deposited in the Cambridge Crystallographic Data Center (CCDC) with the following accession numbers: **2**-A (2348712). These data can be obtained free of charge from the CCDC at https://www.ccdc.cam.ac.uk/structures/.

SUPPLEMENTAL INFORMATION

Supplemental information can be found online at https://doi.org/10.1016/j.chempr.2024.06.033.

ACKNOWLEDGMENTS

This material is based upon work supported by the Air Force Office of Scientific Research under award number FA9550-22-1-0254. G.G.D.H. acknowledges the NSF CAREER award (DMR-2142887), Alfred P. Sloan Foundation (FG-2022-18328), and the Camille and Henry Dreyfus Foundation (TC-23-028). Some PXRD patterns were obtained on a powder X-ray diffractometer funded by AFOSR DURIP award (FA9550-23-1-0072). The solid-state NMR spectrometer used in this project was funded by the National Science Foundation Major Research Instrumentation Program (award 1726346), and the solution-state NMR spectrometer by the NIH Shared Instrumentation Program (1S10OD034395). K.E.S. acknowledges the Sustainable Futures Initiative Grant Program: Early Career Postdoctoral-Faculty Bridge grant #67848-ECP of the ACS Campaign for a Sustainable Futures, which provided support for S.M.T. We gratefully acknowledge Prof. Steven Lopez at Northeastern University and Prof. Ken Houk at UCLA for the discussions on the computation of anthracenes and dianthracenes.

AUTHOR CONTRIBUTIONS

S. Chakraborty, C.R., G.S., and S. Cho synthesized and characterized all compounds and performed ^{1}H and ^{13}C NMR, solution-state UV-vis spectroscopy, TGA, and DSC analysis of the compounds. H.P.Q.N. performed IR imaging of the heat cascade and the analysis of activation energies. J.U. provided quantum chemical calculations and contributed to the mechanistic understanding. J.Y.C. and J.P. conducted crystal structure simulation based on PXRD. Z.S. and K.S.-R. performed solid-state NMR analysis of compounds. Q.Q. acquired solid-state UV-vis absorption spectra.

S.M.T. and K.E.S. guided IR-laser-triggering experiments. G.G.D.H. conceived the project, designed the experiments, and refined the manuscript. All authors discussed the results and edited the manuscript.

DECLARATION OF INTERESTS

The authors filed a US provisional application related to this work.

Received: April 18, 2024
Revised: June 3, 2024
Accepted: June 25, 2024
Published: July 22, 2024

REFERENCES

1. Orrego-Hernández, J., Dreos, A., and Moth-Poulsen, K. (2020). Engineering of Norbornadiene/Quadricyclane Photoswitches for Molecular Solar Thermal Energy Storage Applications. Acc. Chem. Res. *53*, 1478–1487. https://doi.org/10.1021/acs.accounts.0c00235.

2. Jorner, K., Dreos, A., Emanuelsson, R., El Bakouri, O., Fdez. Galván, I., Börjesson, K., Feixas, F., Lindh, R., Zietz, B., Moth-Poulsen, K., and Ottosson, H. (2017). Unraveling factors leading to efficient norbornadiene–quadricyclane molecular solar-thermal energy storage systems. J. Mater. Chem. A *5*, 12369–12378. https://doi.org/10.1039/C7TA04259K.

3. Kunz, A., Heindl, A.H., Dreos, A., Wang, Z., Moth-Poulsen, K., Becker, J., and Wegner, H.A. (2019). Intermolecular London Dispersion Interactions of Azobenzene Switches for Tuning Molecular Solar Thermal Energy Storage Systems. ChemPlusChem *84*, 1145–1148. https://doi.org/10.1002/cplu.201900330.

4. Le, M., and Han, G.G.D. (2022). Stimuli-Responsive Organic Phase Change Materials: Molecular Designs and Applications in Energy Storage. Acc. Mater. Res. *3*, 634–643. https://doi.org/10.1021/accountsmr.2c00049.

5. Wang, Z., Losantos, R., Sampedro, D., Morikawa, M.-a., Börjesson, K., Kimizuka, N., and Moth-Poulsen, K. (2019). Demonstration of an azobenzene derivative based solar thermal energy storage system. J. Mater. Chem. A *7*, 15042–15047. https://doi.org/10.1039/C9TA04905C.

6. Dong, L., Feng, Y., Wang, L., and Feng, W. (2018). Azobenzene-based solar thermal fuels: design, properties, and applications. Chem. Soc. Rev. *47*, 7339–7368. https://doi.org/10.1039/C8CS00470F.

7. Qiu, Q., Yang, S., Gerkman, M.A., Fu, H., Aprahamian, I., and Han, G.G.D. (2022). Photon Energy Storage in Strained Cyclic Hydrazones: Emerging Molecular Solar Thermal Energy Storage Compounds. J. Am. Chem. Soc. *144*, 12627–12631. https://doi.org/10.1021/jacs.2c05384.

8. Wang, Z., Udmark, J., Börjesson, K., Rodrigues, R., Roffey, A., Abrahamsson, M., Nielsen, M.B., and Moth-Poulsen, K. (2017). Evaluating Dihydroazulene/Vinylheptafulvene Photoswitches for Solar Energy Storage Applications. ChemSusChem *10*, 3049–3055. https://doi.org/10.1002/cssc.201700679.

9. Brøndsted Nielsen, M., Ree, N., Mikkelsen, K.V., and Cacciarini, M. (2020). Tuning the dihydroazulene – vinylheptafulvene couple for storage of solar energy. Russ. Chem. Rev. *89*, 573–586. https://doi.org/10.1070/RCR4944.

10. Kanai, Y., Srinivasan, V., Meier, S.K., Vollhardt, K.P.C., and Grossman, J.C. (2010). Mechanism of Thermal Reversal of the (Fulvalene) tetracarbonyldiruthenium Photoisomerization: Toward Molecular Solar–Thermal Energy Storage. Angew. Chem. Int. Ed. Engl. *49*, 8926–8929. https://doi.org/10.1002/anie.201002994.

11. Lennartson, A., Lundin, A., Börjesson, K., Gray, V., and Moth-Poulsen, K. (2016). Tuning the photochemical properties of the fulvalene-tetracarbonyl-diruthenium system. Dalton Trans. *45*, 8740–8744. https://doi.org/10.1039/C6DT01343K.

12. Kean, Z.S., Akbulatov, S., Tian, Y., Widenhoefer, R.A., Boulatov, R., and Craig, S.L. (2014). Photomechanical Actuation of Ligand Geometry in Enantioselective Catalysis. Angew. Chem. Int. Ed. Engl. *53*, 14508–14511. https://doi.org/10.1002/anie.201407494.

13. Zheng, L.-Q., Yang, S., Lan, J., Gyr, L., Goubert, G., Qian, H., Aprahamian, I., and Zenobi, R. (2019). Solution Phase and Surface Photoisomerization of a Hydrazone Switch with a Long Thermal Half-Life. J. Am. Chem. Soc. *141*, 17637–17645. https://doi.org/10.1021/jacs.9b07057.

14. Helmy, S., Oh, S., Leibfarth, F.A., Hawker, C.J., and Read de Alaniz, J. (2014). Design and Synthesis of Donor–Acceptor Stenhouse Adducts: A Visible Light Photoswitch Derived from Furfural. J. Org. Chem. *79*, 11316–11329. https://doi.org/10.1021/jo502206g.

15. Helmy, S., Leibfarth, F.A., Oh, S., Poelma, J.E., Hawker, C.J., and Read de Alaniz, J. (2014). Photoswitching Using Visible Light: A New Class of Organic Photochromic Molecules. J. Am. Chem. Soc. *136*, 8169–8172. https://doi.org/10.1021/ja503016b.

16. Nishimura, R., Fujisawa, E., Ban, I., Iwai, R., Takasu, S., Morimoto, M., and Irie, M. (2022). Turn-on mode fluorescent diarylethene containing neopentyl substituents that undergoes all-visible-light switching. Chem. Commun. (Camb) *58*, 4715–4718. https://doi.org/10.1039/D2CC00554A.

17. Calbo, J., Weston, C.E., White, A.J.P., Rzepa, H.S., Contreras-García, J., and Fuchter, M.J. (2017). Tuning Azoheteroarene Photoswitch Performance through Heteroaryl Design. J. Am. Chem. Soc. *139*, 1261–1274. https://doi.org/10.1021/jacs.6b11626.

18. Shao, B., Qian, H., Li, Q., and Aprahamian, I. (2019). Structure Property Analysis of the Solution and Solid-State Properties of Bistable Photochromic Hydrazones. J. Am. Chem. Soc. *141*, 8364–8371. https://doi.org/10.1021/jacs.9b03932.

19. Wang, J., Avram, L., Diskin-Posner, Y., Białek, M.J., Stawski, W., Feller, M., and Klajn, R. (2022). Altering the Properties of Spiropyran Switches Using Coordination Cages with Different Symmetries. J. Am. Chem. Soc. *144*, 21244–21254. https://doi.org/10.1021/jacs.2c08901.

20. Gemen, J., Church, J.R., Ruoko, T.-P., Durandin, N., Białek, M.J., Weißenfels, M., Feller, M., Kazes, M., Odaybat, M., Borin, V.A., et al. (2023). Disequilibrating azobenzenes by visible-light sensitization under confinement. Science *381*, 1357–1363. https://doi.org/10.1126/science.adh9059.

21. Klajn, R. (2014). Spiropyran-based dynamic materials. Chem. Soc. Rev. *43*, 148–184. https://doi.org/10.1039/C3CS60181A.

22. Thaggard, G.C., Park, K.C., Lim, J., Maldeni Kankanamalage, B.K.P., Haimerl, J., Wilson, G.R., McBride, M.K., Forrester, K.L., Adelson, E.R., Arnold, V.S., et al. (2023). Breaking the photoswitch speed limit. Nat. Commun. *14*, 7556. https://doi.org/10.1038/s41467-023-43405-w.

23. Williams, D.E., Martin, C.R., Dolgopolova, E.A., Swifton, A., Godfrey, D.C., Ejegbavwo, O.A., Pellechia, P.J., Smith, M.D., and Shustova, N.B. (2018). Flipping the Switch: Fast Photoisomerization in a Confined Environment. J. Am. Chem. Soc. *140*, 7611–7622. https://doi.org/10.1021/jacs.8b02994.

24. Martin, C.R., Park, K.C., Leith, G.A., Yu, J., Mathur, A., Wilson, G.R., Gange, G.B., Barth, E.L., Ly, R.T., Manley, O.M., et al. (2022). Stimuli-Modulated Metal Oxidation States in Photochromic MOFs. J. Am. Chem. Soc. *144*, 4457–4468. https://doi.org/10.1021/jacs.1c11984.

25. Thaggard, G.C., Maldeni Kankanamalage, B.K.P., Park, K.C., Haimerl, J., Fischer, R.A., and Shustova, N.B. (2024). Switching in harmony: Tailoring the properties of functional materials

with orthogonal stimuli. Chemical Physics Reviews. Chemical Physics Reviews *5*, 11305. https://doi.org/10.1063/5.0189069.

26. Gerkman, M.A., Gibson, R.S.L., Calbo, J., Shi, Y., Fuchter, M.J., and Han, G.G.D. (2020). Arylazopyrazoles for Long-Term Thermal Energy Storage and Optically Triggered Heat Release below 0 °C. J. Am. Chem. Soc. *142*, 8688–8695. https://doi.org/10.1021/jacs.0c00374.

27. Han, G.G.D., Deru, J.H., Cho, E.N., and Grossman, J.C. (2018). Optically-regulated thermal energy storage in diverse organic phase-change materials. Chem. Commun. (Camb) *54*, 10722–10725. https://doi.org/10.1039/C8CC05919E.

28. Zhang, Z.-Y., He, Y., Wang, Z., Xu, J., Xie, M., Tao, P., Ji, D., Moth-Poulsen, K., and Li, T. (2020). Photochemical Phase Transitions Enable Coharvesting of Photon Energy and Ambient Heat for Energetic Molecular Solar Thermal Batteries That Upgrade Thermal Energy. J. Am. Chem. Soc. *142*, 12256–12264. https://doi.org/10.1021/jacs.0c03748.

29. Qiu, Q., Qi, Q., Usuba, J., Lee, K., Aprahamian, I., and Han, G.G.D. (2023). Visible light activated energy storage in solid-state Azo-BF2 switches. Chem. Sci. *14*, 11359–11364. https://doi.org/10.1039/D3SC03465H.

30. Sinnwell, M.A., and MacGillivray, L.R. (2016). Halogen-Bond-Templated [2+2] Photodimerization in the Solid State: Directed Synthesis and Rare Self-Inclusion of a Halogenated Product. Angew. Chem. Int. Ed. Engl. *55*, 3477–3480. https://doi.org/10.1002/anie.201510912.

31. Sinnwell, M.A., Baltrusaitis, J., and MacGillivray, L.R. (2015). Combination of Argentophilic and Perfluorophenyl-Perfluorophenyl Interactions Supports a Head-to-Head [2 + 2] Photodimerization in the Solid State. Cryst. Growth Des. *15*, 538–541. https://doi.org/10.1021/cg501571u.

32. Sinnwell, M.A., Groeneman, R.H., Ingenthron, B.J., Li, C., and MacGillivray, L.R. (2021). Supramolecular construction of a cyclobutane ring system with four different substituents in the solid state. Commun. Chem. *4*, 60. https://doi.org/10.1038/s42004-021-00493-3.

33. Biradha, K., and Santra, R. (2013). Crystal engineering of topochemical solid state reactions. Chem. Soc. Rev. *42*, 950–967. https://doi.org/10.1039/C2CS35343A.

34. Rath, B.B., and Vittal, J.J. (2022). Photoreactive Crystals Exhibiting [2 + 2] Photocycloaddition Reaction and Dynamic Effects. Acc. Chem. Res. *55*, 1445–1455. https://doi.org/10.1021/acs.accounts.2c00107.

35. Cho, S., Usuba, J., Chakraborty, S., Li, X., and Han, G.G.D. (2023). Solid-state photon energy storage via reversible [2+2] cycloaddition of donor-acceptor styrylpyrylium system. Chem *9*, 3159–3171. https://doi.org/10.1016/j.chempr.2023.06.007.

36. Qiu, Q., Gerkman, M.A., Shi, Y., and Han, G.G.D. (2021). Design of phase-transition molecular solar thermal energy storage compounds: compact molecules with high energy densities. Chem. Commun. (Camb) *57*, 9458–9461. https://doi.org/10.1039/D1CC03742K.

37. Gonzalez, A., Odaybat, M., Le, M., Greenfield, J.L., White, A.J.P., Li, X., Fuchter, M.J., and Han, G.G.D. (2022). Photocontrolled Energy Storage in Azobispyrazoles with Exceptionally Large Light Penetration Depths. J. Am. Chem. Soc. *144*, 19430–19436. https://doi.org/10.1021/jacs.2c07537.

38. Schulte, R., Afflerbach, S., Paululat, T., and Ihmels, H. (2023). Bis- and Tris-norbornadienes with High Energy Densities for Efficient Molecular Solar Thermal Energy Storage. Angew. Chem. Int. Ed. Engl. *62*, e202309544. https://doi.org/10.1002/anie.202309544.

39. Dreos, A., Wang, Z., Udmark, J., Ström, A., Erhart, P., Börjesson, K., Nielsen, M.B., and Moth-Poulsen, K. (2018). Liquid Norbornadiene Photoswitches for Solar Energy Storage. Adv. Energy Mater. *8*, 1703401. https://doi.org/10.1002/aenm.201703401.

40. Quant, M., Lennartson, A., Dreos, A., Kuisma, M., Erhart, P., Börjesson, K., and Moth-Poulsen, K. (2016). Low Molecular Weight Norbornadiene Derivatives for Molecular Solar-Thermal Energy Storage. Chemistry *22*, 13265–13274. https://doi.org/10.1002/chem.201602530.

41. Sarathy, S.M., Tingas, E.-A., Nasir, E.F., Detogni, A., Wang, Z., Farooq, A., and Im, H. (2019). Three-stage heat release in n-heptane auto-ignition. Proc. Combust. Inst. *37*, 485–492. https://doi.org/10.1016/j.proci.2018.07.075.

42. Slovetsky, D.I. (1988). Mechanisms of decomposition of hydrocarbons in electrical discharges. Pure Appl. Chem. *60*, 753–768. https://doi.org/10.1351/pac198860050753.

43. Paciorek, K.L., and Kratzer, R.H. (1970). Electric discharge reactions of hydrocarbons. Can. J. Chem. *48*, 1777–1779. https://doi.org/10.1139/v70-291.

44. Li, Q., Shen, H.-X., Liu, C., Wang, C.-F., Zhu, L., and Chen, S. (2022). Advances in frontal polymerization strategy: From fundamentals to applications. Prog. Polym. Sci. *127*, 101514. https://doi.org/10.1016/j.progpolymsci.2022.101514.

45. Suslick, B.A., Hemmer, J., Groce, B.R., Stawiasz, K.J., Geubelle, P.H., Malucelli, G., Mariani, A., Moore, J.S., Pojman, J.A., and Sottos, N.R. (2023). Frontal Polymerizations: From Chemical Perspectives to Macroscopic Properties and Applications. Chem. Rev. *123*, 3237–3298. https://doi.org/10.1021/acs.chemrev.2c00686.

46. Bansal, K., Pojman, J.A., Webster, D., and Quadir, M. (2020). Frontal Polymerization of a Thin Film on a Wood Substrate. ACS Macro Lett. *9*, 169–173. https://doi.org/10.1021/acsmacrolett.9b00887.

47. Robertson, I.D., Hernandez, H.L., White, S.R., and Moore, J.S. (2014). Rapid Stiffening of a Microfluidic Endoskeleton via Frontal Polymerization. ACS Appl. Mater. Interfaces *6*, 18469–18474. https://doi.org/10.1021/am5061596.

48. Shi, Y., Gerkman, M.A., Qiu, Q., Zhang, S., and Han, G.G.D. (2021). Sunlight-activated phase change materials for controlled heat storage and triggered release. J. Mater. Chem. A *9*, 9798–9808. https://doi.org/10.1039/D1TA01007G.

49. Zhitomirsky, D., Cho, E., and Grossman, J.C. (2016). Solid-State Solar Thermal Fuels for Heat Release Applications. Adv. Energy Mater. *6*, 1502006. https://doi.org/10.1002/aenm.201502006.

50. Greenfield, J.L., Gerkman, M.A., Gibson, R.S.L., Han, G.G.D., and Fuchter, M.J. (2021). Efficient Electrocatalytic Switching of Azoheteroarenes in the Condensed Phases. J. Am. Chem. Soc. *143*, 15250–15257. https://doi.org/10.1021/jacs.1c06359.

51. Sun, C.-L., Wang, C., and Boulatov, R. (2019). Applications of Photoswitches in the Storage of Solar Energy. ChemPhotoChem *3*, 268–283. https://doi.org/10.1002/cptc.201900030.

52. Garcia-Garibay, M.A. (2007). Molecular Crystals on the Move: From Single-Crystal-to-Single-Crystal Photoreactions to Molecular Machinery. Angew. Chem. Int. Ed. Engl. *46*, 8945–8947. https://doi.org/10.1002/anie.200702443.

53. Awad, W.M., Davies, D.W., Kitagawa, D., Mahmoud Halabi, J., Al-Handawi, M.B., Tahir, I., Tong, F., Campillo-Alvarado, G., Shtukenberg, A.G., Alkhidir, T., et al. (2023). Mechanical properties and peculiarities of molecular crystals. Chem. Soc. Rev. *52*, 3098–3169. https://doi.org/10.1039/D2CS00481J.

54. Tong, F., Xu, W., Al-Haidar, M., Kitagawa, D., Al-Kaysi, R.O., and Bardeen, C.J. (2018). Photomechanically Induced Magnetic Field Response by Controlling Molecular Orientation in 9-Methylanthracene Microcrystals. Angew. Chem. Int. Ed. Engl. *57*, 7080–7084. https://doi.org/10.1002/anie.201802423.

55. Tong, F., Hanson, M.P., and Bardeen, C.J. (2016). Analysis of reaction kinetics in the photomechanical molecular crystal 9-methylanthracene using an extended Finke–Watzky model. Phys. Chem. Chem. Phys. *18*, 31936–31945. https://doi.org/10.1039/C6CP04459J.

56. Kim, T., Zhu, L., Mueller, L.J., and Bardeen, C.J. (2014). Mechanism of Photoinduced Bending and Twisting in Crystalline Microneedles and Microribbons Composed of 9-Methylanthracene. J. Am. Chem. Soc. *136*, 6617–6625. https://doi.org/10.1021/ja412216z.

57. Easley, C.J., Tong, F., Dong, X., Al-Kaysi, R.O., and Bardeen, C.J. (2020). Using light intensity to control reaction kinetics and reversibility in photomechanical crystals. Chem. Sci. *11*, 9852–9862. https://doi.org/10.1039/D0SC03557B.

58. Zhu, L., Tong, F., Salinas, C., Al-Muhanna, M.K., Tham, F.S., Kisailus, D., Al-Kaysi, R.O., and Bardeen, C.J. (2014). Improved Solid-State Photomechanical Materials by Fluorine Substitution of 9-Anthracene Carboxylic Acid. Chem. Mater. *26*, 6007–6015. https://doi.org/10.1021/cm502866e.

59. Zhu, L., Al-Kaysi, R.O., Dillon, R.J., Tham, F.S., and Bardeen, C.J. (2011). Crystal Structures and Photophysical Properties of 9-Anthracene Carboxylic Acid Derivatives for Photomechanical Applications. Cryst. Growth Des. *11*, 4975–4983. https://doi.org/10.1021/cg200883b.

60. Gately, T.J., Sontising, W., Easley, C.J., Islam, I., Al-Kaysi, R.O., Beran, G.J.O., and Bardeen, C.J. (2021). Effect of halogen substitution on energies and dynamics of reversible photomechanical crystals based on 9-anthracenecarboxylic acid. CrystEngComm *23*, 5931–5943. https://doi.org/10.1039/D1CE00846C.

61. Sun, C., Oppenheim, J.J., Skorupskii, G., Yang, L., and Dincă, M. (2022). Reversible topochemical polymerization and depolymerization of a crystalline 3D porous organic polymer with C–C bond linkages. Chem *8*, 3215–3224. https://doi.org/10.1016/j.chempr.2022.07.028.

62. Kory, M.J., Wörle, M., Weber, T., Payamyar, P., van de Poll, S.W., Dshemuchadse, J., Trapp, N., and Schlüter, A.D. (2014). Gram-scale synthesis of two-dimensional polymer crystals and their structure analysis by X-ray diffraction. Nat. Chem. *6*, 779–784. https://doi.org/10.1038/nchem.2007.

63. Kissel, P., Murray, D.J., Wulftange, W.J., Catalano, V.J., and King, B.T. (2014). A nanoporous two-dimensional polymer by single-crystal-to-single-crystal photopolymerization. Nat. Chem. *6*, 774–778. https://doi.org/10.1038/nchem.2008.

64. Collet, G., Lathion, T., Besnard, C., Piguet, C., and Petoud, S. (2018). On-Demand Degradation of Metal–Organic Framework Based on Photocleavable Dianthracene-Based Ligand. J. Am. Chem. Soc. *140*, 10820–10828. https://doi.org/10.1021/jacs.8b05047.

65. Huang, X.-D., Hong, B.-K., Wen, G.-H., Li, S.-H., and Zheng, L.-M. (2023). Photo-controllable heterostructured crystals of metal–organic frameworks via reversible photocycloaddition. Chem. Sci. *14*, 1852–1860. https://doi.org/10.1039/D2SC06732C.

66. Ganguly, G., Sultana, M., and Paul, A. (2018). Designing Efficient Solar-Thermal Fuels with [n.n](9,10)Anthracene Cyclophanes: A Theoretical Perspective. J. Phys. Chem. Lett. *9*, 328–334. https://doi.org/10.1021/acs.jpclett.7b03170.

67. Nishiuchi, T., Kisaka, K., and Kubo, T. (2021). Synthesis of Anthracene-Based Cyclic π-Clusters and Elucidation of their Properties Originating from Congested Aromatic Planes. Angew. Chem. Int. Ed. Engl. *60*, 5400–5406. https://doi.org/10.1002/anie.202013349.

68. Manring, L.E., Peters, K.S., Jones, G., II, and Bergmark, W.R. (1985). Observation of a common intermediate in the photocycloaddition and photocycloreversion of linked anthracenes. J. Am. Chem. Soc. *107*, 1485–1489. https://doi.org/10.1021/ja00292a006.

69. Bergmark, W.R., Jones, G., II, Reinhardt, T.E., and Halpern, A.M. (1978). Photoisomerization of bis(9-anthryl)methane and other linked anthracenes. The role of excimers and biradicals in photodimerization. J. Am. Chem. Soc. *100*, 6665–6673. https://doi.org/10.1021/ja00489a018.

70. Jones, G., Reinhardt, T.E., and Bergmark, W.R. (1978). Photon energy storage in organic materials— The case of linked anthracenes. Sol. Energy *20*, 241–248. https://doi.org/10.1016/0038-092X(78)90103-2.

71. Brancart, J., Van Damme, J., Du Prez, F., and Van Assche, G. (2021). Substituent effect on the thermophysical properties and thermal dissociation behaviour of 9-substituted anthracene derivatives. Phys. Chem. Chem. Phys. *23*, 2252–2263. https://doi.org/10.1039/D0CP05953F.

72. Bouas-Laurent, H., Desvergne, J.-P., Castellan, A., and Lapouyade, R. (2001). Photodimerization of anthracenes in fluid solutions: (part 2) mechanistic aspects of the photocycloaddition and of the photochemical and thermal cleavage. Chem. Soc. Rev. *30*, 248–263. https://doi.org/10.1039/B006013P.

73. Grimme, S., Peyerimhoff, S.D., Bouas-Laurent, H., Desvergne, J.-P., Becker, H.-D., Sarge, S.M., and Dreeskamp, H. (1999). Calorimetric and quantum chemical studies of some photodimers of anthracenes. Phys. Chem. Chem. Phys. *1*, 2457–2462. https://doi.org/10.1039/A900965E.

74. Donati, D., Guarini, G.G.T., and Sarti-Fantoni, P. (1991). DSC Investigation on anthracene derivative photodimers. J. Therm. Anal. *37*, 1917–1922. https://doi.org/10.1007/BF01912223.

75. Van Damme, J., Vlaminck, L., Van Assche, G., Van Mele, B., van den Berg, O., and Du Prez, F. (2016). Synthesis and evaluation of 9-substituted anthracenes with potential in reversible polymer systems. Tetrahedron *72*, 4303–4311. https://doi.org/10.1016/j.tet.2016.05.077.

76. Van Damme, J., van den Berg, O., Brancart, J., Van Assche, G., and Du Prez, F. (2019). A novel donor-π-acceptor anthracene monomer: Towards faster and milder reversible dimerization. Tetrahedron *75*, 912–920. https://doi.org/10.1016/j.tet.2019.01.007.

77. Donati, D., Guarini, G., and Sarti-Fantoni, P. (1972). Thermal Behaviour and Monomerization Kinetics of 9-CN Anthracene and 9-CN, 10-Acetoxy Anthracene Dimers in the Solid State. Mol. Cryst. Liq. Cryst. *17*, 187–195. https://doi.org/10.1080/15421407208083167.

78. Schmidt, G.M.J. (1971). Photodimerization in the solid state. Pure Appl. Chem. *27*, 647–678. https://doi.org/10.1351/pac197127040647.

79. Salzillo, T., Zaccheroni, S., Della Valle, R.G., Venuti, E., and Brillante, A. (2014). Micro Raman Investigation of the Photodimerization Reaction of 9-Cyanoanthracene in the Solid State. J. Phys. Chem. C *118*, 9628–9635. https://doi.org/10.1021/jp412484x.

80. Theocharis, C.R., and Jones, W. (1984). The thermally induced phase transition of crystalline 9-cyanoanthracene dimer: a single crystal study. J. Chem. Soc. Chem. Commun. 369–370. https://doi.org/10.1039/C39840000369.

81. Nishiuchi, T., Makihara, Y., Kishi, R., Sato, H., and Kubo, T. (2023). Stacked antiaromaticity in the π-congested space between the aromatic rings in the anthracene dimer. J. Phys. Org. Chem. *36*, e4451. https://doi.org/10.1002/poc.4451.